Editors' Suggestion

Shubnikov–de Haas oscillations in two-dimensional hole gases with competing cyclotron and Zeeman energy

Davide Costa, Lucas E. A. Stehouwer, Davide Degli Esposti, and Giordano Scappucci*
QuTech and Kavli Institute of Nanoscience, Delft University of Technology, Lorentzweg 1, 2628 CJ Delft, Netherlands

(Received 22 September 2025; revised 20 February 2026; accepted 2 March 2026; published 19 March 2026)

Evaluation of the quantum lifetime in two-dimensional hole systems, together with band-structure parameters such as the effective mass and g factor, becomes challenging when competing energy scales shape Shubnnikov–de Haas oscillations in a magnetic field. Here, we overcome this challenge for holes with pseudospin $J_z = \pm\frac{3}{2}$, confined in low-disorder strained germanium quantum wells. We extract self-consistently the effective mass, g factor, and quantum lifetime, and estimate a maximum quantum mobility of $133(3) \times 10^3$ cm^2/V s, setting a benchmark for holes in group IV semiconductors. The high quality of the hole gas if further highlighted by observing clean fractional quantum Hall states at low magnetic field and density.

DOI: 10.1103/pc57-schm

I. INTRODUCTION

Semiconductor two-dimensional channels are an archetype platform for the development of quantum technology based on spin qubits in quantum dots [1] and superconductor-semiconductor hybrid devices [2]. The disorder potential in these quantum devices is typically proxied by measurements of charge mobility and percolation-induced critical density of the parent two-dimensional (2D) electron or hole gas. A careful analysis of the Shubnikov–de Haas (SdH) oscillations of the magnetoresistivity as a function of temperature T and carrier density p [3] may extract other relevant channel properties, such as the quantum lifetime τ_q [4], together with the in-plane effective mass m^*, the associated quantum quantum mobility $\mu_q = e\tau_q/m^*$, and the out-of-plane effective g factor (g^*). However, the evaluation of these parameters within the validity of the theoretical approximations is challenged by the competition among the energy scales associated with orbital motion, Zeeman spin splitting, spin-orbit interaction, subband splittings, and collisional level broadening.

This challenge is particularly pronounced in two-dimensional hole gases (2DHG) in strained Ge quantum wells (QWs), recently emerged as a compelling platform for the development of quantum information processing devices [5]. In strained Ge QWs, the valence band ground state has predominantly heavy-hole symmetry [6] (pseudospin $J_z = \pm 3/2$) with a remarkably light in-plane effective mass ($\sim 0.055 m_0$) [7,8] and large out-of-plane g^* (~ 20) at the Γ point, based on the Luttinger parameters of Ge [9]. Conversely, the in-plane component of g^* is close to zero, giving rise to a very strong g^* anisotropy [5]. If the 2DHG carrier density is sufficiently low and close to the Γ point, these peculiar valence band states give rise to competing cyclotron energy ($E_C = \frac{\hbar e}{m^* m_0} B$) and Zeeman energy ($E_Z = g^* \mu_B B$) even at low magnetic fields B. Previous experimental studies [10–15] have highlighted the unconventional low-density regime where E_Z overcomes the orbital Landau level quantization energy gap $E_{orb} = E_C - E_Z$. In this regime, SdH oscillations minima for odd (spin-split) filling factors prevail over the even minima at low magnetic fields. This early spin splitting makes a reliable evaluation of m^*, g^*, and τ_q, related to the disorder-induced collisional level broadening $\Gamma = \hbar/2\tau_q$ [16], inconvenient within standard theoretical frameworks [3,14]. Furthermore, the coincidence method [17], successfully applied in 2D electron systems [18,19] for extracting g^*, does not work with holes in Ge, due to the strong g^* anisotropy and the nonparabolic band structure.

In this paper, we exploit recent advancements in strained Ge QWs with exceptionally low disorder to advance the evaluation of the critical parameters m^*, g^*, and τ_q self-consistently, across the $E_{orb} \simeq E_Z$ transition, and at a single measurement temperature, overcoming a long-standing challenge for 2DHGs with heavy-hole symmetry.

II. RESULTS

We measure at a temperature $T = 100$ mK the Ge/SiGe heterostructure field effect transistor studied in Ref. [20] with an ultrahigh mobility of $4.4(2) \times 10^6$ cm^2/V s and a low percolation density of $4.5(1) \times 10^9$ cm^{-2}. A top-view image of a similar device is provided in Ref. [21]. The low disorder in the channel allows us to measure high-quality low-field SdH oscillations in the longitudinal resistivity $\rho_{xx}(B)$ down to low density and establish our theoretical framework. We first consider in Fig. 1(a) the oscillatory magnetoresistance $\Delta\rho_{xx}(B)$ [22] computed following the approach adopted in previous studies of high-mobility Ge [23]—measured at a special crossover density p^* where oscillation minima for

*Contact author: g.scappucci@tudelft.nl

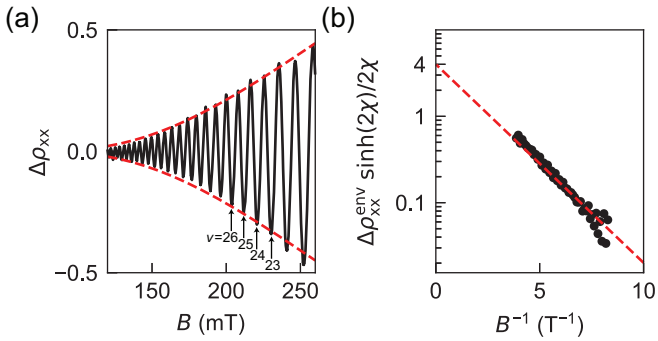

FIG. 1. (a) Oscillatory component of the longitudinal resistivity $\Delta\rho_{xx}$ (solid black curve) at low magnetic fields B after background subtraction. The measurements are performed at a crossover density p^* of 1.28×10^{11} cm^{-2}, where oscillation minima for even and odd filling factor ν are observed with equal prominence, implying equal orbital and Zeeman energy gaps. The red dashed curves are the analytical envelope obtained from a single-harmonic approximation, assuming a Lorentzian density of states. (b) Corresponding Dingle plot of the normalized envelope amplitude $\Delta\rho_{xx}^{env}\sinh(2\chi)/2\chi$ vs B^{-1} and linear fit (red dashed line).

even and odd filling factor ν are observed with equal prominence. In our device, this condition is achieved by fine-tuning the applied gate voltage to set the channel carrier density to 1.28×10^{11} cm^{-2}. Under the assumption of a Lorentzian density of states (DOS), and neglecting effects such as structure inversion asymmetry (specifically Rashba splitting) and chemical potential oscillations, the oscillatory component of the normalized longitudinal resistivity can be expressed as a sum over harmonics l, following Ref. [24],

$$\Delta\rho_{xx}(B) = 4\sum_{l=1}^{\infty} e^{-l\frac{\pi}{\omega_c\tau_q}} \frac{l\chi}{\sinh(l\chi)} \times \cos\left[2\pi l\left(\frac{hp}{2eB} - \frac{1}{2}\right)\right]\cos\left(l\frac{\pi}{2}g^*m^*\right), \quad (1)$$

where $\omega_c = eB/m^*m_0$ is the cyclotron angular frequency and $\chi = 2\pi^2 k_B T/\hbar\omega_c$ is the temperature-dependent coefficient. The measurements in Fig. 1(a) imply the condition $E_{orb} \simeq E_Z$, corresponding to $g^*m^* = 1$, under which the odd harmonics of $\Delta\rho_{xx}(B)$ in Eq. (1) are suppressed due to the $\cos(l\frac{\pi}{2})$ term. Since the higher-order harmonics ($l \geqslant 4$) are exponentially attenuated, we approximate Eq. (1) to the first even harmonic $l = 2$ and obtain for the envelope of $\Delta\rho_{xx}$ the expression

$$\Delta\rho_{xx}^{env}(B) \approx 4e^{-2\frac{\pi}{\omega_c\tau_q}} \frac{2\chi}{\sinh(2\chi)}. \quad (2)$$

We use this analytical formula to fit the envelope of the experimental oscillations in Fig. 1(a) assuming, in this first analysis, an effective mass of $0.055m_0$ [8]. This assumption implies $g^* = 1/m^* = 18.2$ at this special crossover density p^*. The fit (dashed red lines) shows good agreement with the measured data, supporting the validity of the single-harmonic approximation in this regime. Figure 1(b) shows the corresponding Dingle plot [3] and its linear fit (dashed red line), from which we extract a τ_q of 3.71(3) ps. The minor splitting in the experimental data at low fields is attributed to residual $l = 1$ harmonics which decay slower than the dominant $l = 2$ term. Notably, the fit intercepts the y axis at a value of 4, consistent with the prediction from the analytical expression in Eq. (2). This validates our initial assumption of a Lorentzian DOS, confirming our theoretical framework.

We now extend our analysis to the broader range of carrier densities, above or below the crossover density, where the product g^*m^* deviates from unity due to the nonparabolicity of the valence bands and the varying degree of heavy-hole–light-hole mixing.

Figures 2(a), 2(d), 2(g), and 2(j) illustrate the energy-level diagrams of the 2DHG at four representative densities: 1.59, 1.28, 0.99, and 0.71×10^{11} cm^{-2}. The highest density corresponds to the common condition $E_Z < E_{orb}$, i.e., $g^*m^* < 1$ [Fig. 2(a)]. At the intermediate density p^*, the same considered for Fig. 1(a), the two energy gaps have equal amplitude [Fig. 2(d)] and $g^*m^* = 1$, marking a transition point in the system's energy hierarchy [Fig. 2(d)]. Finally, at the two lowest densities the Zeeman gap exceeds the orbital gap and $g^*m^* > 1$ [Figs. 2(g)–2(j)].

The corresponding SdH oscillations shown in Figs. 2(b), 2(e), 2(h), and 2(k) illustrate how the interplay between Zeeman and orbital energy gaps governs the onset and relative strength of quantum oscillations. To characterize the effects of the competing energy scales, we define B_O and B_Z as the magnetic field values at which the oscillations corresponding to the orbital and Zeeman gap first appear, respectively. At high density [Fig. 2(b)], where $E_{orb} > E_Z$, the condition $B_O < B_Z$ is observed: oscillations first emerge from the orbital gap overcoming the disorder broadening Γ, and even filling factors dominate. At the crossover density [Fig. 2(e)], $B_O \approx B_Z$, indicating that both gaps contribute equally and oscillations for even and odd filling factors have comparable amplitude. At lower densities [Figs. 2(h) and 2(k)], the order is reversed, $B_O > B_Z$: oscillations originate first from the Zeeman gap, and odd filling factors become stronger. Figures 2(c), 2(f), 2(i), and 2(l) show a first satisfactory theoretical fit of the oscillatory magnetoresistance for the four densities. Similarly to the analysis in Fig. 1, we have assumed a constant effective mass $m^*_{i=0} = 0.055m_0$, but differently we use the generalized harmonic expansion of Eq. (1).

Building on this first fit, Fig. 3(a) illustrates the self-consistent fitting loop we introduce to extract in a quantitative way the three metrics g^*, m^*, and τ_q as a function of density p. For this study, we enforce a linear relationship between m^* and p, building on previous experiments with strained Ge QWs [7,25,26]. This choice is nonrestrictive, as the feedback loop can be used to explore alternative density-mass dependencies. The linear mass-density relationship is then nested into the theoretical connection between g^* and m^*, peculiar to states with heavy-hole symmetry and derived from the Luttinger Hamiltonian [26,27],

$$|g_\perp| = 2\left(-3K + (\gamma_1 + \gamma_2) - \frac{m_0}{m^*}\right), \quad (3)$$

where $\gamma_1 = 13.38$, $\gamma_2 = 4.26$, and $K = 3.41$ are the Luttinger parameters of Ge [9]. The loop proceeds as follows: the first iteration, starting with a constant m^*, yields preliminary values of $g^*_i(p)$ and $\tau_{q_i}(p)$ for each density. Next, these extracted $g^*_i(p)$ values are fitted with the theoretical relation in Eq. (3), from which we obtain a linear dependence of

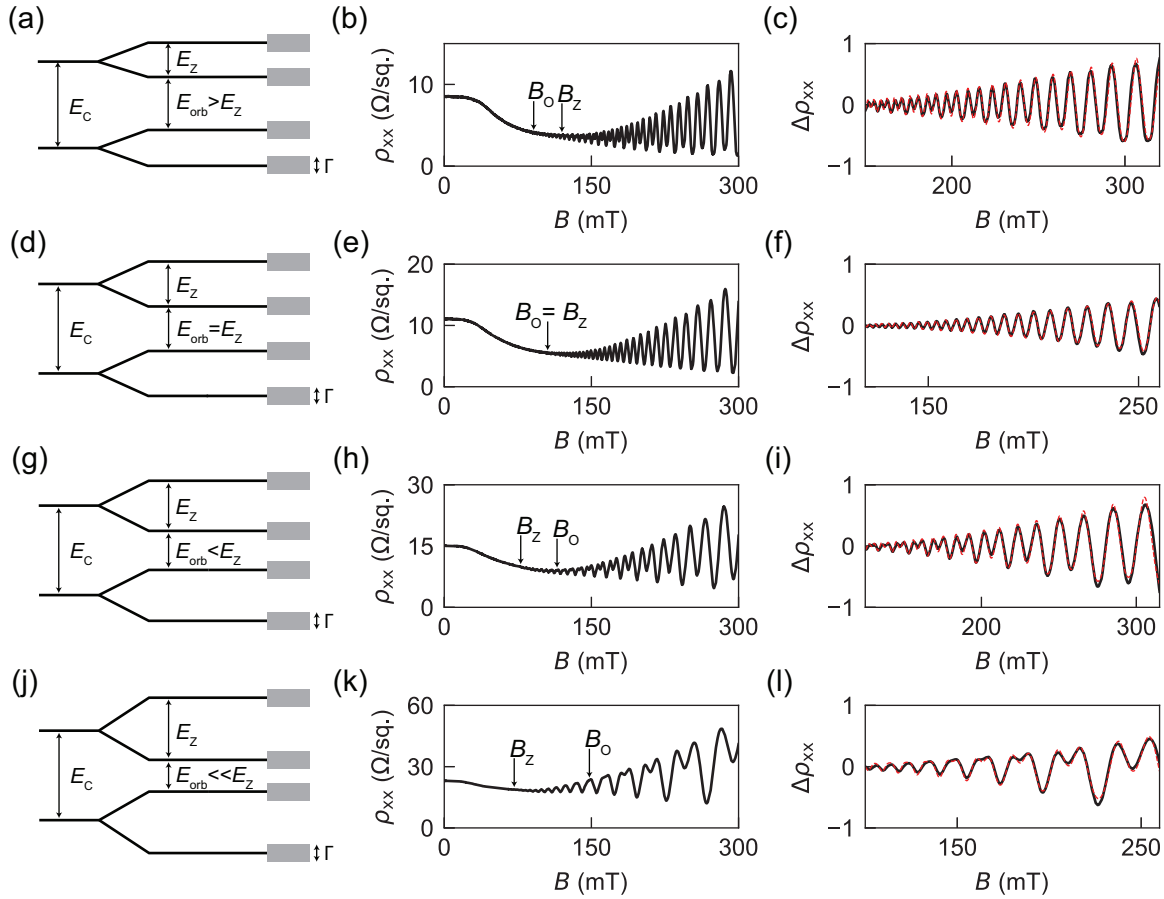

FIG. 2. (a), (d), (g), (j) Landau-level ladders of the two-dimensional hole gas in a quantizing perpendicular magnetic field, highlighting the interplay between Zeeman and orbital energy for the four measured densities: (a) $p_{2D} = 1.59 \times 10^{11}$ cm^{-2}, $E_Z > E_{orb}$; (d) $p_{2D} = 1.28 \times 10^{11}$ cm^{-2}, $E_Z = E_{orb}$; (g) $p_{2D} = 0.99 \times 10^{11}$ cm^{-2}, $E_Z < E_{orb}$; (j) $p_{2D} = 0.71 \times 10^{11}$ cm^{-2}, $E_Z \ll E_{orb}$. (b), (e), (h), (k) Shubnikov–de Haas oscillations of the longitudinal resistivity ρ_{xx} at low magnetic field values, corresponding to the energy ladders and density in (a), (d), (g), (j), respectively. B_O and B_Z mark the magnetic fields for the onset of quantum oscillations corresponding to the orbital and Zeeman gap, respectively. (c), (f), (i), (l) Normalized longitudinal resistivity oscillatory component $\Delta\rho_{xx}$ (solid black curves) obtained from (a), (d), (g), (j), respectively. Dashed red curves are numerical fits using Eq. (1).

m_i^* on the density. The updated values $m_i^*(p)$ are then fed back into Eq. (1) to refine the fit, producing new sets of values for the parameters $g_i^*(p)$ and $\tau_{q_i}(p)$. This procedure is repeated iteratively until the discrepancy ε between the fitted $g_i^*(p)$ and the mass-dependent $g^*[m_i^*(p)]$ is below a threshold of 10^{-2}.

The outcome of this self-consistent fitting procedure is summarized in Figs. 3(b)–3(d). The estimated density-dependent effective mass m^* [Fig. 3(b)], with the linear relationship with density imposed *a priori*, are in line with experiments [7] at higher densities and our extrapolated zero-density mass of $0.0486(1)m_0$ is within 12% of the theoretical prediction ($0.055m_0$) at the Γ point [8]. The estimated density-dependent g^* [Fig. 3(c), black points] are in good agreement with the theoretical relationship from Eq. (3) [Fig. 3(c), red dashed line]. The validation of g^* and m^* with previous reports and theoretical expectations brings confidence on the constraints of our framework. This enables the reliable extraction of the quantum transport figure of merit τ_q [Fig. 3(d)], despite the complex harmonic mixing in the oscillations, along with the quantum mobility $\mu_q = e\tau_q/m^*$. At the highest density of 1.59×10^{11} cm^{-2} we obtain a remarkable τ_q of 5.5(1) ps, corresponding to a small energy level broadening $\Gamma = 60$ μeV and a μ_q of $137(1) \times 10^3$ cm^2/V s. Differently than transport time and mobility, these metrics are sensitive to scattering through all angles and are indicative of the high quality of the heterostructure [16]. Furthermore, the quantum mobility sets a benchmark for holes in group IV semiconductors, improving previous qualitative estimates in the 25–84 $\times 10^3$ cm^2/V s range measured at similar densities [13,15,28].

The high quantum mobility, indicative of the low-disorder environment in the 2DHG, allows for the observation of an extensive sequence of fractional quantum Hall states at higher magnetic fields, as evidenced by the longitudinal resistivity ρ_{xx} (top panel) and normalized Hall conductivity σ_{xy} (bottom panel) plotted in Fig. 4 as functions of the filling factor ν for three different carrier densities (1.28, 0.99, and 0.71 $\times 10^{11}$ cm^{-2}). Pronounced minima in ρ_{xx} and corresponding quantized plateaus in σ_{xy} are clearly visible at several fractional filling factors of the even denominator series, including $\nu = 1/3$, 2/3, 2/5, 3/5, 3/7, and 4/7. The clear observation of these fractional quantum Hall states at relatively low magnetic fields, with the first fractional state $\nu = 2/3$ appearing at fields as low as 5 T for a density of 0.71×10^{11} cm^{-2},

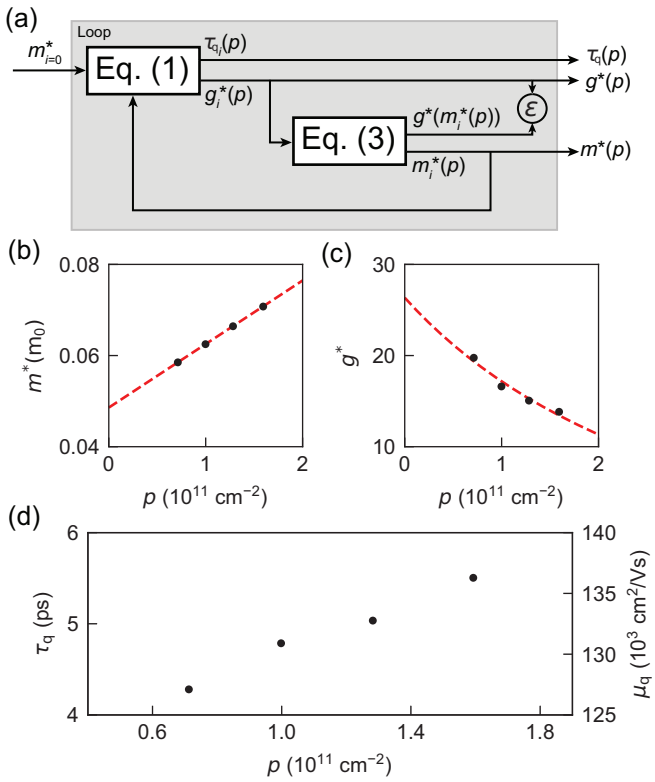

FIG. 3. (a) Flowchart of the self-consisting loop for fitting the density-dependent oscillatory component of the magnetoresistance $\Delta\rho_{xx}$ in Fig. 2 using the generalized harmonic expansion of Eq. (1). As an output we obtain the density-dependent effective mass $m^*(p)$, effective g factor $g^*(p)$, and quantum lifetime τ_q. Equation (3) relates $g^*(p)$ and $m^*(p)$, the latter assumed proportional to p. (b) Extracted density-dependent m^* (black dots) with linear fit (red dashed line). (c) Extracted density-dependent g^* (black dots) with a theoretical dependence from Eq. (3) (red dashed line). (d) Extracted density-dependent τ_q (black dots, left axis) and corresponding quantum mobility μ_q (right axis). Error bars represent fit uncertainties.

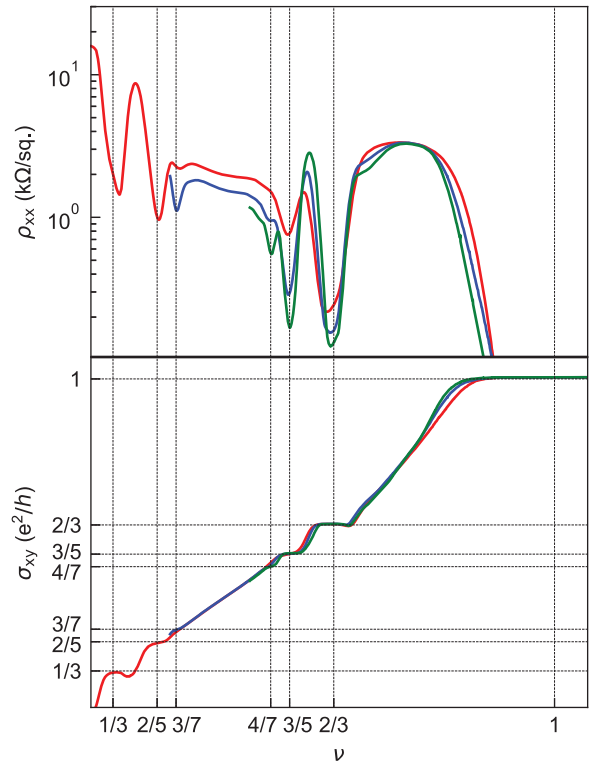

FIG. 4. Longitudinal resistivity ρ_{xx} (top) and normalized transverse conductivity σ_{xy} (bottom) as a function of filling factor ν for $\nu < 1$, measured at three different densities: 0.71×10^{11} cm^{-2} (solid red lines), 0.99×10^{11} cm^{-2} (solid blue lines), and 1.28×10^{11} cm^{-2} (solid green lines). For each curve, the filling factors are obtained via the quantum Hall relationship $\nu = hp/eB$, where h is the Planck constant.

underscores the remarkable electronic and material quality of the 2DHG.

III. CONCLUSIONS

In summary, we have developed a self-consistent framework to reliably extract the in-plane m^*, out-of-plane g^*, and τ_q in strained Ge quantum wells, overcoming the challenge posed by competing cyclotron and Zeeman energy scales in 2DHGs with heavy-hole symmetry. Leveraging ultralow-disorder Ge/SiGe heterostructures, we accessed the unconventional regime where spin splitting dominates over orbital quantization and demonstrated agreement between experiment and theory using a Lorentzian DOS model for disorder broadening. The high quantum mobility and the observation of clean fractional quantum Hall states highlight the electronic quality of the platform. Our results establish strained Ge quantum wells as a rich system for exploring spin physics in 2D hole gases, with direct implications for quantum device applications.

ACKNOWLEDGMENTS

This research was supported by the European Union through the Horizon 2020 research and innovation programme under the Grant Agreement No. 951852 (QLSI) and the Horizon Europe Framework Programme under grant agreement No. 101069515 (IGNITE). This work was supported by the Netherlands Organisation for Scientific Research (NWO/OCW), via the Open Competition Domain Science - M program. This research was sponsored in part by The Netherlands Ministry of Defence under Awards No. R23/009.

The views, conclusions, and recommendations contained in this document are those of the authors and are not necessarily endorsed nor should they be interpreted as representing the official policies, either expressed or implied, of The Netherlands Ministry of Defence. The Netherlands Ministry of Defence is authorized to reproduce and distribute reprints for Government purposes notwithstanding any copyright notation herein.

DATA AVAILABILITY

The data that support the findings of this article are openly available [29].

[1] G. Burkard, T. D. Ladd, A. Pan, J. M. Nichol, and J. R. Petta, Semiconductor spin qubits, Rev. Mod. Phys. **95**, 025003 (2023).

[2] E. Prada, P. San-Jose, M. W. A. De Moor, A. Geresdi, E. J. H. Lee, J. Klinovaja, D. Loss, J. Nygård, R. Aguado, and L. P. Kouwenhoven, From Andreev to Majorana bound states in hybrid superconductor–semiconductor nanowires, Nat. Rev. Phys. **2**, 575 (2020).

[3] P. T. Coleridge, Small-angle scattering in two-dimensional electron gases, Phys. Rev. B **44**, 3793 (1991).

[4] S. Das Sarma and F. Stern, Single-particle relaxation time versus scattering time in an impure electron gas, Phys. Rev. B **32**, 8442 (1985).

[5] G. Scappucci, C. Kloeffel, F. A. Zwanenburg, D. Loss, M. Myronov, J.-J. Zhang, S. De Franceschi, G. Katsaros, and M. Veldhorst, The germanium quantum information route, Nat. Rev. Mater. **6**, 926 (2021).

[6] R. Winkler, *Spin-Orbit Coupling Effects in Two-Dimensional Electron and Hole Systems*, Springer Tracts in Modern Physics Vol. 191 (Springer, Berlin, 2003).

[7] M. Lodari, A. Tosato, D. Sabbagh, M. A. Schubert, G. Capellini, A. Sammak, M. Veldhorst, and G. Scappucci, Light effective hole mass in undoped Ge/SiGe quantum wells, Phys. Rev. B **100**, 041304(R) (2019).

[8] L. A. Terrazos, E. Marcellina, Z. Wang, S. N. Coppersmith, M. Friesen, A. R. Hamilton, X. Hu, B. Koiller, A. L. Saraiva, D. Culcer, and R. B. Capaz, Theory of hole-spin qubits in strained germanium quantum dots, Phys. Rev. B **103**, 125201 (2021).

[9] P. Lawaetz, Valence-band parameters in cubic semiconductors, Phys. Rev. B **4**, 3460 (1971).

[10] T. M. Lu, C. T. Harris, S. H. Huang, Y. Chuang, J. Y. Li, and C. W. Liu, Effective g factor of low-density two-dimensional holes in a Ge quantum well, Appl. Phys. Lett. **111**102108 (2017).

[11] T. M. Lu, L. A. Tracy, D. Laroche, S.-H. Huang, Y. Chuang, Y.-H. Su, J.-Y. Li, and C. W. Liu, Density-controlled quantum Hall ferromagnetic transition in a two-dimensional hole system, Sci. Rep. **7**, 2468 (2017).

[12] M. Lodari, O. Kong, M. Rendell, A. Tosato, A. Sammak, M. Veldhorst, A. R. Hamilton, and G. Scappucci, Lightly strained germanium quantum wells with hole mobility exceeding one million, Appl. Phys. Lett. **120**, 122104 (2022).

[13] L. E. Stehouwer, A. Tosato, D. Degli Esposti, D. Costa, M. Veldhorst, A. Sammak, and G. Scappucci, Germanium wafers for strained quantum wells with low disorder, Appl. Phys. Lett. **123**, 092101 (2023).

[14] M. Myronov, J. Kycia, P. Waldron, W. Jiang, P. Barrios, A. Bogan, P. Coleridge, and S. Studenikin, Holes outperform electrons in group IV semiconductor materials, Small Sci. **3**, 2200094 (2023).

[15] M. Myronov, P. Waldron, P. Barrios, A. Bogan, and S. Studenikin, Electric field-tuneable crossing of hole Zeeman splitting and orbital gaps in compressively strained germanium semiconductor on silicon, Commun. Mater. **4**, 104 (2023).

[16] S. Das Sarma and E. H. Hwang, Mobility versus quality in two-dimensional semiconductor structures, Phys. Rev. B **90**, 035425 (2014).

[17] F. F. Fang and P. J. Stiles, Effects of a tilted magnetic field on a two-dimensional electron gas, Phys. Rev. **174**, 823 (1968).

[18] G. M. Minkov, V. Y. Aleshkin, O. E. Rut, A. A. Sherstobitov, S. A. Dvoretski, N. N. Mikhailov, and A. V. Germanenko, Anisotropy of the in-plane *g*-factor of electrons in HgTe quantum wells, Phys. Rev. B **101**, 085305 (2020).

[19] Z. Lei, C. A. Lehner, K. Rubi, E. Cheah, M. Karalic, C. Mittag, L. Alt, J. Scharnetzky, P. Märki, U. Zeitler, W. Wegscheider, T. Ihn, and K. Ensslin, Electronic *g* factor and magnetotransport in InSb quantum wells, Phys. Rev. Res. **2**, 033213 (2020).

[20] D. Costa, L. E. A. Stehouwer, Y. Huang, S. Martí-Sánchez, D. Degli Esposti, J. Arbiol, and G. Scappucci, Reducing disorder in Ge quantum wells by using thick SiGe barriers, Appl. Phys. Lett. **125**, 222104 (2024).

[21] A. Sammak, D. Sabbagh, N. W. Hendrickx, M. Lodari, B. Paquelet Wuetz, A. Tosato, L. Yeoh, M. Bollani, M. Virgilio, M. A. Schubert, *et al.*, Shallow and undoped germanium quantum wells: A playground for spin and hybrid quantum technology, Adv. Funct. Mater. **29**, 1807613 (2019).

[22] In our measurements, $\Delta\rho_{xx}(B)$ is obtained by subtracting a second-degree polynomial background from the normalized longitudinal magnetoresistivity given by

$$\Delta\rho_{xx_0}(B) = \frac{\rho_{xx}(B) - \rho_{xx}(0)}{\rho_{xx}(0)}.$$

[23] T. Irisawa, M. Myronov, O. A. Mironov, E. H. C. Parker, K. Nakagawa, M. Murata, S. Koh, and Y. Shiraki, Hole density dependence of effective mass, mobility and transport time in strained Ge channel modulation-doped heterostructures, Appl. Phys. Lett. **82**, 1425 (2003).

[24] D. R. Candido, S. I. Erlingsson, H. Gramizadeh, J. V. I. Costa, P. J. Weigele, D. M. Zumbühl, and J. C. Egues, Beating-free quantum oscillations in two-dimensional electron gases with strong spin-orbit and Zeeman interactions, Phys. Rev. Res. **5**, 043297 (2023).

[25] B. Rössner, H. von Känel, D. Chrastina, G. Isella, and B. Batlogg, Effective mass measurement: The influence of hole band nonparabolicity in SiGe/Ge quantum wells, Semicond. Sci. Technol. **22**, S191 (2007).

[26] I. L. Drichko, A. A. Dmitriev, V. Malysh, I. Y. Smirnov, H. von Känel, M. Kummer, D. Chrastina, and G. Isella, Effective g factor of 2D holes in strained Ge quantum wells, J. Appl. Phys. **123**, 165703 (2018).

[27] T. Wimbauer, K. Oettinger, A. L. Efros, B. K. Meyer, and H. Brugger, Zeeman splitting of the excitonic recombination in $In_xGa_{1-x}As/GaAs$ single quantum wells, Phys. Rev. B **50**, 8889 (1994).

[28] M. Lodari, N. W. Hendrickx, W. I. Lawrie, T.-K. Hsiao, L. M. Vandersypen, A. Sammak, M. Veldhorst, and G. Scappucci, Low percolation density and charge noise with holes in germanium, Mater. Quantum Technol. **1**, 011002 (2021).

[29] D. Costa and G. Scappucci, Data Repository for "Quantum oscillations in two-dimensional hole gases with competing cyclotron and Zeeman energy" [Dataset], Zenodo (2025), https://doi.org/10.5281/zenodo.17099877.